

Electronic structure of copper pnictides: Influence of different cations and pnictogens

J. A. McLeod*

Department of Physics and Engineering Physics, University of Saskatchewan, 116 Science Place, Saskatoon, Saskatchewan S7N 5E2, Canada

E. Z. Kurmaev

Institute of Metal Physics, Russian Academy of Sciences—Ural Division, 620990 Yekaterinburg, Russia

I. Perez

Department of Physics and Engineering Physics, University of Saskatchewan, 116 Science Place, Saskatoon, Saskatchewan S7N 5E2, Canada

V. K. Anand, P. Kanchana Perera, and D. C. Johnston

Ames Laboratory and Department of Physics and Astronomy, Iowa State University, Ames, Iowa 50011, USA

A. Moewes

Department of Physics and Engineering Physics, University of Saskatchewan, 116 Science Place, Saskatoon, Saskatchewan S7N 5E2, Canada

(Received 29 April 2013; published 10 July 2013)

We present calculated electronic structures and x-ray emission and absorption spectroscopy measurements of five copper pnictides. The x-ray emission and absorption spectra, which probe the occupied and unoccupied states, respectively, provide an empirical justification of the calculated electronic structure. We therefore verify the prediction that the copper $3d$ states are fully occupied and buried deep in the valence band, and the Fermi surface of these materials is characterized by s, p states. We show that generally the calculated electronic structure is in excellent agreement with our measurements. We finally examine the Fermi surfaces of these pnictides, and suggest that copper antimonides may exhibit efficient Fermi surface nesting similar to iron pnictides.

DOI: [10.1103/PhysRevB.88.014508](https://doi.org/10.1103/PhysRevB.88.014508)

PACS number(s): 71.20.-b, 31.15.E-, 78.70.En, 78.70.Dm

I. INTRODUCTION

Since $\text{La}(\text{O}_{1-x}\text{F}_x)\text{FeAs}$ was found to exhibit superconductivity as a member of an entirely new class of Fe-based superconductors,¹ an immense amount of research has gone into this field.² Superconductivity in these iron pnictides is often dependent on either pressure or doping,³ and it is common to substitute other transition metals for iron to achieve the latter.^{4,5} BaFe_2As_2 , a typical iron pnictide superconductor that is structurally simple and is easily synthesized in large, high-quality crystals,^{6,7} has been shown to exhibit robust superconductivity after substituting iron with cobalt and nickel,^{4,6} but no bulk superconductivity after substituting with copper; magnetic susceptibility measurements of Cu-substituted BaFe_2As_2 show no evidence of superconductivity down to 1.8 K.⁶

However it is not immediately clear why copper should have such a deleterious effect on superconductivity in iron pnictides. Superconductivity has been realized in the copper pnictide LiCu_2P_2 ,⁸ so the presence of copper alone in a pnictide does not rule out superconductivity. Several groups initially studied Co- and Ni-substituted BaFe_2As_2 in the context of adding free carriers to the system in a rigid band model.^{9,10} While this worked well for Co-substituted BaFe_2As_2 , it provided an inadequate explanation for the properties of Ni-substituted BaFe_2As_2 .¹¹

Later theoretical work suggested that the transition-metal substitutions were isovalent with iron,¹² and therefore did not increase (or decrease) the free carriers in the system. These

findings were supported by x-ray spectroscopy measurements which showed the copper in Cu-substituted BaFe_2As_2 possessed a full $3d^{10}$ shell.¹³

Some time ago the electronic structure of BaCu_2As_2 and SrCu_2As_2 was studied with density functional theory (DFT) calculations, as a comparison to the isostructural iron pnictides (and superconducting parent compounds) BaFe_2As_2 and SrFe_2As_2 .¹⁴ These calculations suggested that the Cu $3d$ shell was fully occupied, and these $3d$ states were chemically inert due to their depth in the valence band and weak contribution to the density of states (DOS) at the Fermi level. While we agree that these states are unlikely to dominate the transport properties—unlike, for example, the Fe $3d$ states in iron pnictides which have a major influence at the Fermi level^{12,15–18}—we have previously shown that states relatively deep in the valence band, including those from atoms with full $3d$ shells, can be chemically active.^{13,19} Since the full $3d$ shell is the major difference between Cu and other transition metals in pnictides, and since previous research suggested that the binding energy of the full $3d$ shell of Cu-substituted BaFe_2As_2 was underestimated,¹³ it is worth taking a closer look at the electronic structure of copper pnictides to elucidate the influence of the copper $3d$ states.

Second, while most pnictides involve a pnictide transition metal layer wherein the transition metals form a central plane with the pnictogens staggered above and below this plane, the copper antimonides have two distinct alternating layer structures: a normal one with the transition metals as the

central plane and one with antimony as the central plane. This structure provides two distinct sites for copper, and the copper site in the second type of Cu-Sb plane lacks the approximately tetrahedral coordination that is common for transition metals in these layered pnictides. Since the local geometry has a strong influence on the degeneracies of the $3d$ orbitals and their overlap with ligand states, the presence of these additional sites provides a useful probe of whether the Cu $3d^{10}$ shell really is chemically inert.

Very recent angle-resolved photoelectron spectroscopy (ARPES) measurements of Ni- and Cu-substituted BaFe_2As_2 show that the Ni and Cu $3d$ states are buried progressively deeper in the valence band,²⁰ as was previously predicted with lower resolution x-ray emission spectroscopy (XES).¹³ These recent results provide a clearer demonstration of the inadequacies of the rigid band model to describe the behavior of Ni- and Cu-substituted BaFe_2As_2 ; in particular the Fermi surface volume in both systems is smaller than predicted by the rigid band model, and the critical temperature T_c is dependent not just on the Fermi surface volume but also on the disorder in the system.²⁰

We study the electronic structure of the copper pnictides BaCu_2Sb_2 , SrCu_2Sb_2 , $\text{SrCu}_2(\text{As}_{0.84}\text{Sb}_{0.16})_2$, SrCu_2As_2 , and CaCu_2As_2 using DFT calculations and soft x-ray spectroscopy measurements. DFT calculations have proven to be a useful tool in studying layered pnictides²¹ and are therefore an appropriate aid in analyzing our experimental spectra. X-ray emission and absorption spectroscopy (XES and XAS, respectively) of the Cu $L_{2,3}$ edge provide a local and symmetry-specific probe of the occupied and unoccupied states, respectively. In the soft x-ray regime the radiation field transition operator acts as a dipole operator, and therefore these measurements probe transitions from the Cu $2p$ core levels to the Cu $3d$ levels in the valence (for XES) and conduction (for XAS) bands. Soft x-ray spectroscopy is therefore an ideal technique to probe the copper $3d$ states in these layered pnictides.

II. EXPERIMENTAL AND THEORETICAL METHODS

We performed soft x-ray emission and absorption spectroscopy measurements on crushed single crystals of BaCu_2Sb_2 , SrCu_2Sb_2 , $\text{SrCu}_2(\text{As}_{0.84}\text{Sb}_{0.16})_2$, SrCu_2As_2 , and $\text{CaCu}_{1.7}\text{As}_2$. The crystals were grown with the self-flux technique, as previously reported.^{22,23} We also measured polycrystalline CuO and Cu metal (both Alfa Aesar, 99.9% purity) as references.

Our x-ray emission and absorption spectroscopy measurements were conducted at the Advanced Light Source (ALS) at the Lawrence Berkeley National Laboratories (Berkeley, CA, USA) and at the Canadian Light Source (CLS) at the University of Saskatchewan (Saskatoon, SK, Canada), respectively. A Rowland circle geometry x-ray spectrometer with spherical gratings and an area-sensitive detector was used at Beamline 8.0.1 at the ALS to collect the x-ray emission spectra,²⁴ while a channel plate fluorescence detector on the spherical grating monochromator beamline at the CLS was used to collect the x-ray absorption spectra in bulk-sensitive total fluorescence yield (TFY) mode and surface-sensitive total electron yield (TEY) mode.²⁵ Since both modes produced almost identical spectra, only the TEY measurements are shown here. This

shows that the samples suffered negligible surface oxidation. The measurement resolution was about 10^3 and 2×10^3 for the emission and absorption measurements, respectively. All absorption spectra were normalized to the incident photon current using a highly transparent gold mesh in front of the sample to correct for intensity fluctuations in the incident photon beam. The samples were affixed to a sample plate, placed under ultrahigh vacuum ($\sim 10^{-7}$ to 10^{-8} torr), and measured at room temperature without any further preparation. The relative calibration between XES and XAS measurements was checked by exciting near resonance and observing the energy of the elastic scatter from the incident x-ray beam in the XES spectrometer.

Density functional theory (DFT) calculations were performed using the experimental crystal structures of these copper pnictides.^{22,23} The full-potential linearized augmented plane wave (FP-LAPW) method was used²⁶ implemented by the WIEN2k code.²⁷ We used convergence and basis set parameters that are typical for the types of materials we investigate here.²⁸ For the exchange correlation potential we used the common generalized gradient approximation of Perdew, Burke, and Enzerhof (PBE).²⁹ For copper-deficient $\text{CaCu}_{1.7}\text{As}_2$ we used a $2 \times 2 \times 1$ supercell and removed 2 copper atoms (to make $\text{CaCu}_{1.75}\text{As}_2$, which we deemed sufficiently close to the synthesized material to allow direct comparison). The space group of this copper-deficient structure was $P4_2/mmc$. For $\text{SrCu}_2(\text{As}_{0.84}\text{Sb}_{0.16})_2$, we likewise created a $2 \times 2 \times 1$ supercell [using the basic unit cell with fractional occupancy reported for $\text{SrCu}_2(\text{As}_{0.84}\text{Sb}_{0.16})_2$ in Ref. 23] and replaced two arsenic atoms with antimony to make $\text{SrCu}_2(\text{As}_{0.875}\text{Sb}_{0.125})_2$. The space group of this structure was $Cmc2_1$. These supercell structures were not optimized (either in terms of the lattice constants or the internal atomic positions) because the experimental structures with fractional occupancies were quite accurately determined,^{22,23} and the substitutions or deficiencies in $\text{SrCu}_2(\text{As}_{0.84}\text{Sb}_{0.16})_2$ and $\text{CaCu}_{1.7}\text{As}_2$, respectively, are significant enough (i.e., more than one part in ten) that any significant distortion in the supercell structure would show up in the experimental x-ray diffraction pattern. Finally, band structures and Fermi surfaces were calculated for select copper pnictides. For the band structures 1000 k points were chosen along each path through the first Brillouin zone, while for the Fermi surfaces 100 000 k points were chosen in the first Brillouin zone to ensure a smooth surface with minimal interpolation.

For Cu metal and CuO reference materials, we likewise used the experimental crystal structures.^{30,31} The electronic structure of Cu metal was calculated in the same manner as the pnictides, described above. However it is well known that a simple DFT calculation fails to reproduce the correct electronic structure for CuO,³² so we added an on-site Coulomb potential of 7.8 eV³³ to the Cu $3d$ states and reduced the symmetry of the unit cell so each Cu atom was at an inequivalent site (in an attempt to prevent forcing the system into adopting an unphysical magnetic structure). Calculating the electronic structure of a strongly correlated system can be quite intricate,^{34,35} and we would like to stress that we deem our calculations of CuO to be “accurate” only in the sense that it adequately reproduces the measured Cu L_3 XES spectrum and provides a reasonable band gap (1.9 eV).

The XES and XAS spectra were also simulated from the DFT calculations by multiplying the partial densities of states with the dipole transition probability, implemented in the XSPEC package of WIEN2k.³⁶ The influence of a core hole on the x-ray absorption spectra was examined only for stoichiometric CaCu_2As_2 , using a single Cu $2p_{3/2}$ hole in a $3 \times 3 \times 2$ supercell. [$\text{CaCu}_{1.75}\text{As}_2$ has multiple inequivalent Cu sites, and a separate core hole calculation would be necessary for each site. However since the Cu local environment (i.e., the As coordination) is unaffected by Cu deficiencies, we feel justified in using the simpler core hole calculation on stoichiometric CaCu_2As_2 as a model for the XAS of $\text{CaCu}_{1.75}\text{As}_2$.] In all other systems the core hole was not simulated since it was clear *a posteriori* that the ground-state conduction band provided an adequate representation of the measured x-ray spectra. The calculated x-ray spectra were broadened with a Voigt function to mimic the experimental resolution and lifetime broadening; for XES spectra the lifetime Lorentzian broadening full width at half maximum (FWHM) was 0.6 eV at the Fermi level and 2.0 eV at the bottom of the valence band (increasing quadratically with energy from the Fermi level)³⁷ and the instrumental Gaussian broadening FWHM was 0.9 eV, while for XAS spectra the lifetime Lorentzian broadening FWHM was 0.3 eV at the Fermi level and 1.0 eV at the top of the XAS spectrum and the instrumental Gaussian broadening FWHM was 0.45 eV.

III. RESULTS AND DISCUSSION

A. Density of states

The electronic structure of two copper pnictides (BaCu_2As_2 and SrCu_2As_2) was studied using DFT methods some time ago by Singh, who concluded that the materials were *sp* metals.¹⁴ We have performed similar calculations, using the experimentally obtained structures,^{22,23} for BaCu_2Sb_2 , SrCu_2Sb_2 , SrCu_2As_2 , and $\text{CaCu}_{1.75}\text{As}_2$ as well as copper metal, as shown in Fig. 1. Our calculations show the same trends as those reported by Singh, namely the Cu $3d$ states largely localize into a band between 3 and 5 eV below the Fermi level (E_F), in contrast to Cu metal where the Cu $3d$ states are only about 1.5 eV below E_F . The $3d$ states in Cu metal have an average energy of around 3 eV below E_F , as shown in Fig. 1(f), similar to that in SrCu_2As_2 and BaCu_2As_2 , but in Cu metal, the Cu $3d^{10}$ band has a much broader dispersion than that in the copper pnictides, and there is a much greater amplitude of Cu $3d^{10}$ states at 1.5 eV below E_F in Cu metal than in the copper pnictides. In Fig. 1 we show the electronic density of states (DOS) to lower energies than that shown previously,¹⁴ revealing the same low-energy pnictogen *s* band as found in the iron pnictides,¹⁵ this band being at lower energies for As than for Sb. Also as in the case of the iron pnictides, there is significant pnictogen *p*-, cation *d*-, and copper *s*- and *d*-state hybridization at the bottom of the main valence band, around 6 to 5 eV below the Fermi level. We point out that while there is a broad distribution of pnictogen *p*- and copper *s*-states through the valence band (from -6 eV to E_F at 0 eV),¹⁴ there is also considerable “interstitial” charge in this region. These interstitial states are those which fall outside of the atomic spheres (and are therefore strongly dependent upon the specific

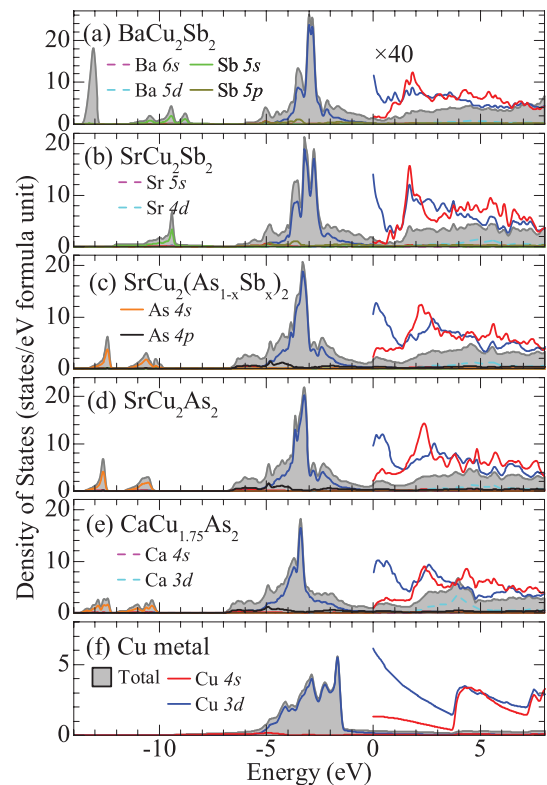


FIG. 1. (Color online) The calculated DOS (sum of both spin channels) versus energy for all copper pnictides studied herein, compared with that of copper metal. The Fermi energy is at 0 eV. The color scheme for the total DOS and the *d*- and *s*-symmetry partial DOS for copper are consistent between all panels. Because of the conduction band states have relatively weak intensity but are important for XAS, the unoccupied Cu $4s$, $3d$ states have been plotted twice, the second time scaled by a factor of 40.

sphere size, unlike, say, the total DOS), but since our sphere sizes were nearly touching the bulk of this interstitial charge must fall outside of the direct axis connecting two adjacent atoms (such as Cu and a pnictogen), and therefore should not be involved with σ -like bonding between the two. This is supportive of the general conclusion that pnictogen-pnictogen bonding (compared to copper-pnictogen bonding) is quite important in these materials.¹⁴

For reference, the total DOS at E_F for the five compounds discussed herein is given in Table I. Note that the highest DOS at E_F occurs in SrCu_2Sb_2 , and even a relatively minor amount of Sb substitution will significantly raise the DOS at E_F [compare $\text{SrCu}_2(\text{As}_{0.875}\text{Sb}_{0.125})_2$ to SrCu_2As_2 in Table I].

The crystal structure of BaCu_2Sb_2 was originally reported to have the tetragonal $I4/mmm$ space group,³⁸ but was recently refined to be orthorhombic $Immm$, and possibly even monoclinic $P21/c$.²³ We calculated the DOS for both the $I4/mmm$ and $Immm$ structures and found very little difference between them—and certainly no differences that would be resolvable with our x-ray measurements. This is not unusual for subtle structural changes in pnictides,¹⁶ and for brevity only the DOS and x-ray spectra from the orthorhombic structure are shown here. (For that matter, the

TABLE I. Calculated total DOS (sum of both spin channels) at E_F for the pnictides and copper metal. Since these systems are nonmagnetic, the spin up and down channels are the same.

Compound	Space Group	Total DOS(E_F) (states/eV formula unit)
CaCu ₂ As ₂	<i>I4/mmm</i>	1.464
CaCu _{1.75} As ₂	<i>P4₂/mmc</i>	1.042
SrCu ₂ As ₂	<i>I4/mmm</i>	1.364
SrCu ₂ (As _{0.875} Sb _{0.125}) ₂	<i>Cmc2₁</i>	1.604
SrCu ₂ Sb ₂	<i>P4/nmm</i>	1.619
BaCu ₂ Sb ₂	<i>I4/mmm</i>	1.440
	<i>Immm</i>	1.465

DOS of CaCu_{1.75}As₂ has essentially the same shape as that of CaCu₂As₂; the major difference is only the location of E_F .)

B. X-ray spectroscopy measurements

To verify the validity of these calculations, we compare x-ray spectra calculated from the ground-state DOS with measured spectra, as shown in Fig. 2. Here the calculated Cu L_3 XES spectrum has been manually shifted in energy to align with the measured spectra (in all cases the calculation underestimates the Cu $2p_{3/2}$ binding energy by about 3.6 eV), and the calculated Cu L_3 XAS spectrum has been shifted accordingly. Because only the XES spectra are aligned, any disagreement in the energies of the calculated and measured XAS spectra reflect differences between the calculated and actual electronic structures.

The Cu L_3 XES spectra are all broad and featureless, which is typical for metal L_3 XES in pnictides.^{13,15} Our calculated XES spectra agree nicely with the measured spectra, but given that the calculated spectra were broadened considerably to match the experimental spectra we should not expect any fine details of the electronic structure to be apparent. Still, the lack of secondary features in the experimental XES spectra of the pnictides shows that the Cu $3d$ states do not hybridize with ligand states outside of the relatively narrow $3d$ band, as suggested by our DOS calculations (refer back to Fig. 1). In contrast, the XES spectrum from CuO [Fig. 2(g)] shows both a low-energy shoulder at 925 eV and a high-energy shoulder at 935 eV, reflecting strong hybridizations with O $2p$ states in these energy ranges.³²

The Cu L_3 XAS spectra are also rather featureless, which is again typical for metal L_3 XAS in pnictides.³⁹ We stress that our XAS calculations used the ground-state electronic structure; since the final state of the XAS transition includes a hole in the Cu $2p_{3/2}$ core state one might expect XAS to measure unoccupied states that are significantly perturbed from the true ground-state conduction band. However the agreement between both the spectral shape and the energy of the measured and calculated Cu L_3 XAS in copper metal is excellent [Fig. 2(a)]; in the metal the highly mobile valence electrons are able to screen the unoccupied core level to the extent that the measured XAS is very close to the true ground-state conduction band. This is in contrast to the metal $L_{2,3}$ XAS of many transition-metal oxides, where the

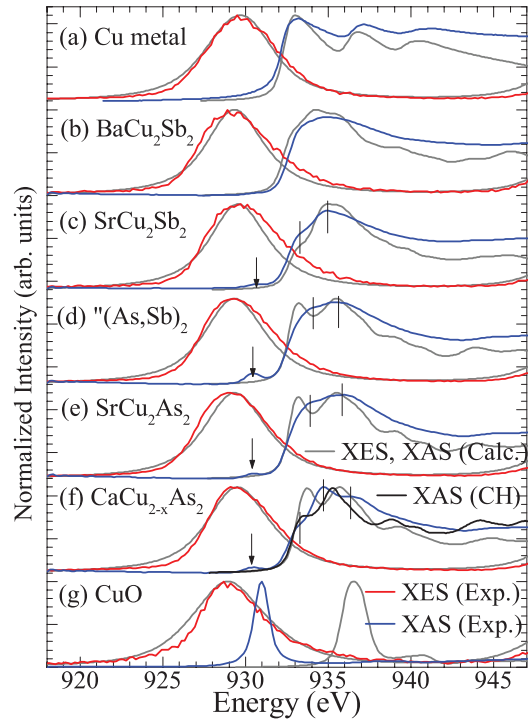


FIG. 2. (Color online) The measured and calculated Cu L_3 XES and XAS for all pnictides studied herein, compared with those for copper metal and CuO. In all cases the XES spectrum was excited at 1000 eV, far above resonance. The calculated XES spectra have been aligned with the measured spectra, with the calculated XAS spectra shifted accordingly. The vertical arrows indicate a small amount of $3d$ holes in the conduction band from surface oxidation. The spectrum set (d), labeled as (As,Sb)₂, corresponds to measured SrCu₂(As_{0.84}Sb_{0.16})₂ and calculated SrCu₂(As_{0.875}Sb_{0.125})₂ spectra, while the spectrum set (f), labeled as CaCu_{2-x}As₂, corresponds to measured CaCu_{1.7}As₂ and calculated CaCu_{1.75}As₂ spectra. All measured XAS spectra were acquired in surface-sensitive total electron yield (TEY) mode, save for the copper metal spectrum which was collected in bulk-sensitive total fluorescence yield (TFY) mode, due to surface oxidation. The Cu L_2 XES band is situated near 949 eV, just off the right edge of the plot. Since the Cu L_2 XES band shows no additional features in either the calculated or measured spectra, it has been omitted for clarity. The same is true for the Cu L_2 XAS band, situated near 955 eV.

unoccupied core level in the final state of the x-ray transition significantly perturbs the unoccupied states to the extent that the measured XAS can be quite different from the ground state (i.e., unperturbed) conduction band.⁴⁰ It is, for example, immediately obvious that the calculated Cu L_3 XAS spectrum of CuO differs quite a bit from the energy of the measured spectrum, as expected since there is a significant core hole shift in the metal $L_{2,3}$ edge XAS spectra in strongly correlated transition-metal oxides.⁴¹ In fact, it is well known that the $L_{2,3}$ XAS spectra of transition metals in strongly correlated oxides bear little resemblance to the ground-state electronic DOS.⁴²

Examining the Cu L_3 XAS spectra of the pnictides, one can immediately see that the copper $3d$ shell is fully occupied, as was previously suggested.^{14,22,23} If there were any holes in the copper $3d$ shell, a sharp $2p \rightarrow 3d$ resonance line would appear on the absorption edge, as is clearly evident in the Cu L_3 XAS

of the typical $3d^9$ system CuO [Fig. 2(g)]. Indeed, since the XAS spectra of the pnictides shown here were collected in the surface-sensitive total electron yield (TEY) mode, there is a small amount of surface oxidation visible by a weak $3d$ resonance indicated by the arrows in Fig. 2. It is therefore clear from these spectra that the copper $3d$ shell is fully occupied in these pnictides.

The previously reported Cu L_3 XAS of Cu-doped BaFe₂As₂ suggests a similar conclusion, but in that case the XAS spectrum is almost identical to that of copper metal.¹³ The Cu in doped iron pnictides seems to be “more metallic” (at least in terms of the distribution of electronic states in the valence and conduction bands resembling that in a pure metal) than the Cu in these copper pnictides, since in the latter case while the XAS is still primarily $2p \rightarrow 4s$ transitions, due to the fully occupied $3d$ shell, the distribution of these unoccupied $4s$ states is rather different from that in copper metal. In particular there is a significant peak right at the bottom of the conduction band (whereas the XAS in copper metal is closer to a simple step function) suggesting a copper-ligand antibonding orbital with prominent $4s$ character.

The agreement in the spectral shapes of the calculated and measured XAS spectra for the pnictides is quite good in the case of BaCu₂Sb₂ [Fig. 2(b)], with both the measured and calculated spectra being relatively featureless. For SrCu₂Sb₂ [Fig. 2(c)] both the measured and calculated XAS spectra show a low-energy shoulder at 933.2 eV and a main peak at 935 eV, although there is a small difference in the relative intensities of these features in the calculated XAS compared to the measured XAS spectrum [see the vertical lines in Fig. 2(c)]. A two-peak structure appears in the calculated XAS spectra for SrCu₂(As_{0.84}Sb_{0.16})₂ and SrCu₂As₂. This fine structure is present, but much less distinct, in the measured spectra for SrCu₂As₂ and SrCu₂(As_{0.84}Sb_{0.16})₂ [see the vertical lines in Figs. 2(d) and 2(e); these lines denote the maximum and the noticeable shoulders in the near-edge measured XAS spectrum].

The measured XAS spectrum for CaCu_{1.7}As₂, however, does not show the same fine structure as the calculated XAS spectrum [of CaCu_{1.75}As₂; see Fig. 2(f)]. The calculated spectrum is very similar to that of SrCu₂As₂, but the measured spectrum shows three distinct features rather than two [see the vertical lines in Fig. 2(f)]. One might think that the measured XAS spectrum should be somewhat “washed out”; the Cu vacancies in CaCu_{1.7}As₂ were perfectly periodic in our calculations, but at room temperature (the conditions of our x-ray measurements) these vacancies are randomly distributed in the real sample.²² However the XAS spectrum of CaCu_{1.7}As₂ is no broader than the XAS spectra from the other copper pnictides, and in fact the explanation for the observed differences is the influence of the core hole (calculated here for stoichiometric CaCu₂As₂, so we do not expect perfect agreement with our measurements of CaCu_{1.7}As₂); when an explicit core hole is included in the calculation the resulting XAS shows the same three features found in the measurement [Fig. 2(f)]. We would like to stress that in this situation the core hole does not influence the energy of the absorption edge; that is still quite close to the ground state E_F . The influence of the core hole in CaCu₂As₂ is merely to rearrange somewhat the unoccupied levels near E_F .

From these data one could make a qualitative argument that the agreement between calculated and measured spectra becomes somewhat worse as the cations and ligands decrease in atomic number; the valence and conduction bands become less “rigid” with the lighter cations and ligands, and the copper $2p_{3/2}$ core hole has a progressively greater distortion on the conduction band. This effect has previously been demonstrated in binary oxides.¹⁹ Finally, the origin of the peaks in the calculated XAS spectra is fairly clear with the unoccupied DOS (refer back to Fig. 1). In all copper pnictides (as well as Cu metal) the main $3d^{10}$ band has a long “tail” that crosses the Fermi level; this forms the first peak (or shoulder) in the Cu L_3 XAS spectrum. At higher energies (around 2–2.5 eV for the copper pnictides, or 4 eV for Cu metal) the unoccupied Cu states are roughly evenly split between hybridized $3d$ and $4s$ states; this forms the second peak in the spectrum of Cu metal and the main peak in the spectrum of the copper pnictides.

C. Identifying valence structures in Cu L_3 XES

Because the Cu L_3 XES from all the copper pnictides (and even that from copper metal) are so similar and so broad, to examine the occupied states probed by these measurements we subtract the “metallic” part from the spectrum; that is, we subtract the measured Cu L_3 XES of copper metal from the measured pnictide spectrum. We scale the copper metal spectrum as much as possible such that the resulting difference spectrum does not have any regions with negative intensity in the L_3 band. (For our purposes here we are only concerned with the L_3 part of the spectrum, so we allow the difference near the L_2 part to be negative.) Since the different materials may have slightly different binding energies, we use the alignment with the calculated XES to convert the energy scale so that it corresponds to that of the DOS (as shown in Fig. 1, this was done by subtracting the shift required to align the calculated XES spectra with the measured ones). The resulting spectra for some of the pnictides are shown in Fig. 3, showing the “metal” and “nonmetal” portions of the spectrum (the sum of these two portions will make the complete pnictide spectrum, as shown in Fig. 2). The “nonmetal” portion of the pnictide L_3 XES shows that the pnictides have a larger quantity of $3d$ states deeper in the valence band than copper metal (about 1 to 1.5 eV lower than the bulk of the Cu $3d$ states in copper metal), in agreement with the calculated DOS (see Fig. 1). Indeed, applying this technique to the spectrum of CuO shows very little “metal” quality in the CuO spectrum (as shown in Fig. 3).

We should point out that the calculated XES (and XAS) spectra for the copper pnictides, taken with respect to the (material-specific) calculated binding energy of the Cu $2p_{3/2}$ core level, needed to be only shifted by an additional 3.5 eV to 3.7 eV⁴³ to match the experimental spectra. Therefore, while our method of aligning the calculated and measured spectra is not terribly precise, because the shifts for Cu metal and the copper pnictides were all were within a spread of 0.2 eV, this method of aligning the Cu L_3 XES spectra to the DOS energy scale should be accurate to within that same amount. As shown in Fig. 3, our argument still applies if the DOS energy scale of the pnictides is changed by ± 0.1 relative to the DOS scale of Cu metal.

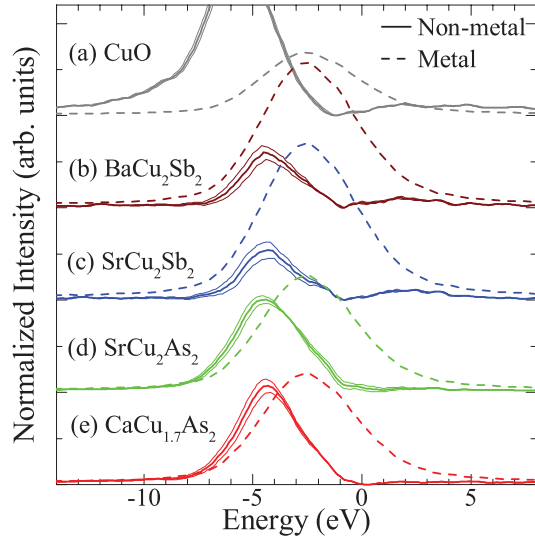


FIG. 3. (Color online) The measured Cu L_3 XES (excited at 1000 eV, far above resonance) of several pnictides and CuO aligned to the Fermi level using the calculated spectra. In each case the solid “nonmetal” line corresponds to removal of as much of the measured Cu L_3 XES of copper metal as possible (after the copper metal spectrum was also aligned to the Fermi level) without allowing the spectral intensity to become negative. The dotted “metal” line corresponds to the amount of the copper metal spectrum that was removed. The sum of the two lines reproduces the original measured spectra shown in Fig. 2. The thinner solid lines correspond to the “nonmetal” if the Fermi level of the copper pnictides was changed by ± 0.1 eV relative to the Fermi level of Cu metal; this demonstrates that the trends shown here are not dependent on the energy alignment within the estimated margin of error.

The relative weighting of the “metal” and “nonmetal” portions of the spectrum also shows that the pnictides with lighter cations and ligands have a larger proportion of “nonmetal” character in their spectra. This suggests that the Cu $3d$ states have progressively greater amplitudes deeper in the valence band for the light cation and ligand pnictides (i.e., $\text{CaCu}_{1.7}\text{As}_2$ has a significantly greater amplitude of Cu $3d$ states near -5 eV than in BaCu_2Sb_2). This is weakly shown in the calculated DOS (see Fig. 1), but the differences between the “nonmetal” spectra of $\text{CaCu}_{1.7}\text{As}_2$ and BaCu_2Sb_2 , for example, are much larger than is supported by our DOS calculations. A second point is that since the Cu L_3 XES from the copper antimonides is very close to that from copper metal (as evidenced by the relatively weak “nonmetal” portion of the spectra shown in Fig. 3), the different local geometries of the copper sites in these antimonides (due to the alternating form of the Cu-Sb layers) does not have much impact on the Cu $3d^{10}$ DOS.

This discussion invites another comparison with Cu-doped BaFe_2As_2 . In the doped iron pnictide system it was clear that it was not possible to mutually align the calculated Cu L_3 XES and XAS spectra with the measured XES and XAS spectra by shifting the calculated spectra by a consistent amount, and it was argued that the center of the Cu $3d$ band was 0.7 eV deeper into the valence band than the calculations suggested.¹³ In the present case, one could argue that the Cu $3d$ states should also be somewhat deeper in the valence band for $\text{CaCu}_{1.7}\text{As}_2$

and SrCu_2As_2 than the calculated DOS suggests. Indeed this is supported by the Cu L_3 XAS (refer back to Fig. 2); the initial shoulder in the Cu L_3 XAS spectrum of $\text{CaCu}_{1.7}\text{As}_2$ and SrCu_2As_2 is weaker in the measured spectrum than in the calculated spectrum (even when a core hole is taken into account); however since this feature is due to the long “tail” of the Cu $3d^{10}$ states crossing the Fermi level, if the Cu $3d$ were deeper in the valence band the amplitude of this “tail” would consequently be reduced. It is, however, fairly clear that simple ground-state DFT calculations are adequate to explain the spectra and electronic structures of BaCu_2Sb_2 and SrCu_2Sb_2 .

It is not entirely unexpected that DFT (especially with the PBE function) could underestimate the binding energy of the Cu $3d^{10}$ shell; the binding energy Zn $3d^{10}$ shell in ZnO is also underestimated by DFT.⁴⁴ Although this problem in ZnO can be fixed by adding an on-site Hubbard-like potential that can provide the correct binding energy and localization of the Zn $3d^{10}$ this is perhaps the wrong approach; the Hubbard-like potential is used to correct for the underestimated correlation energies, while the improper binding energy and localization of the Zn $3d^{10}$ states probably stems from DFT’s incomplete cancellation in the exchange energy—a generic Hartree-Fock calculation (where the exact exchange interaction is used) correctly localizes the Zn $3d^{10}$ states.⁴⁵ The copper pnictides, as discussed above and in the next section, are definitely not strongly correlated systems (in the Hubbard-like sense), but it is not unreasonable that DFT’s approximation of the exchange functional leads to underestimating the binding energy of the Cu $3d^{10}$ states. However this is also dependent on the chemistry of the material, since the calculated binding energy of the Cu $3d^{10}$ states in BaCu_2Sb_2 and SrCu_2Sb_2 (and certainly in Cu metal) seems much closer to experiment than in SrCu_2As_2 and $\text{CaCu}_{1.7}\text{As}_2$, and the calculated Cu $3d^{10}$ binding energy for all copper pnictides is closer to experiment than that of Cu-doped BaFe_2As_2 . Therefore in addition to errors in the exchange approximation, simple DFT may also underestimate the amount of As $4p$ -Cu $3d$ hybridization near the bottom of the valence band.

We would like to stress that our use of the terms “metal” and “nonmetal” portions of the Cu L_3 spectrum are merely labels indicating how the *shape* of the pnictide spectrum agrees (or disagrees) with that of copper metal; we are not suggesting that the states responsible for the “metal” (and “nonmetal”) portions are actually more (or less) metallic. However we should mention that the copper pnictides with the Cu L_3 XES spectrum that most resembles that of copper metal (namely BaCu_2Sb_2 and SrCu_2Sb_2) have lower electrical resistivities at 300 K than the other copper pnictides (whose Cu L_3 XES spectrum resembles that of copper metal the least).^{22,23}

D. Indications of weakly correlated Cu $3d$ states

We have thus far omitted the Cu L_2 portion of the XES spectrum from our discussion, since it has the same shape as the Cu L_3 portion of the XES spectrum. However the ratio of the total intensity of the L_2 and L_3 bands (the “ $L_2:L_3$ ratio”) is a useful quantity. One might expect the $L_2:L_3$ ratio to be 1:2, since there are twice as many $2p_{3/2}$ states as $2p_{1/2}$ states. However, holes in the $2p_{1/2}$ level can be filled by

radiationless Coster-Kronig $L_2L_3M_{4,5}$ transitions (in addition to all the other radiative and Auger transitions that could also fill a $2p_{3/2}$ hole).⁴⁶ This process serves to reduce the intensity of the L_2 emission band, and consequently the $L_2:L_3$ ratio is less than 1:2. The key aspect of Coster-Kronig transitions is that they are much stronger in itinerant systems like metals than in systems with strong on-site correlations (like most transition-metal oxides).⁴⁷ This is because systems with strong on-site correlations have localized orbitals (both occupied and unoccupied), and $L_2L_3M_{4,5}$ Coster-Kronig transitions excite a valence electron to the conduction band. Consequently, there is not always a suitable unoccupied orbital (in terms of quantum numbers like ℓ , m , and spin) for an allowed Coster-Kronig transition involving an arbitrary valence, $2p_{3/2}$, and $2p_{1/2}$ state, unlike in an uncorrelated band structure where almost every conduction band state can be projected into a basis that involves at least some contribution from every set of quantum numbers. Indeed, the Coster-Kronig transition rate changes in metallic magnets, as a consequence of the valence and conduction states having different spin distributions.⁴⁸

The entire Cu $L_{2,3}$ XES spectra for the copper pnictides, as well as that from copper metal and CuO, are shown in Fig. 4, where the amplitude of the L_3 band has been normalized. It is clear that the Cu L_2 band in CuO is more intense than that of copper metal, as expected. The $L_2:L_3$ ratios for the copper pnictides all fall between the extremes set by copper metal and CuO, and the copper pnictide $L_2:L_3$ ratio is somewhat closer to that of copper metal than that of CuO (see the inset of Fig. 4). This suggests that the Cu $3d$ states in copper pnictides are weakly or at most moderately correlated, just like the Fe $3d$ states in iron pnictides.^{17,39,49,50} Indeed, the $L_2:L_3$ ratio for Cu-doped BaFe_2As_2 is very similar to that of the copper pnictides.¹³ Finally, it is interesting to point out that the trend

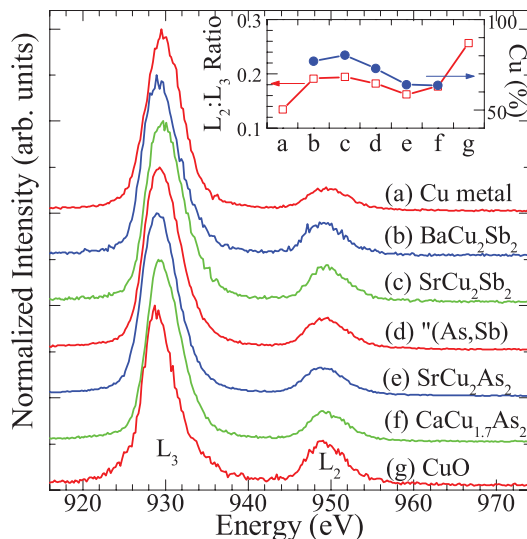


FIG. 4. (Color online) The measured Cu $L_{2,3}$ XES (excited at 1000 eV, far above resonance) for all pnictides studied herein, along with copper metal and CuO. The label (As,Sb) for spectrum (d) refers to $\text{SrCu}_2(\text{As}_{0.84}\text{Sb}_{0.16})_2$. The inset shows the ratio of the integrated intensities of the L_2 and L_3 peaks, and the percentage of Cu L_3 XES from Cu metal that can be subtracted from each pnictide Cu L_3 XES spectrum, as described in Fig. 3.

set by the “metal” portion of the Cu L_3 XES spectra of the copper pnictides (as shown in Fig. 3) is very similar to the trend set by the $L_2:L_3$ ratios for these materials (see the inset of Fig. 4).

E. Band structures and Fermi surfaces

From the perspective of the DOS, there appears to be little difference between As and Sb ligands in these copper pnictides. However the crystal structures are quite different: In the Cu-As compounds there is only one type of Cu-As layer, in which the As are entirely located above and below a Cu plane (the As sites forming the “corrugations” of the Cu-As layer), while there are two types of alternating Cu-Sb layers (one with the Sb forming the “corrugations,” the other with the Cu forming the “corrugations”).²³ If nothing else, the increased number of inequivalent sites suggests a more complicated band structure for the Cu-Sb materials compared to the Cu-As materials.

The band structures of stoichiometric CaCu_2As_2 , SrCu_2As_2 , and SrCu_2Sb_2 near the Fermi level are shown in Fig. 5 (where the labeling nomenclature is according to Ref. 51). Here we use stoichiometric CaCu_2As_2 instead of $\text{CaCu}_{1.75}\text{As}_2$; while the latter is more appropriate since the former cannot be synthesized,²² because $\text{CaCu}_{1.75}\text{As}_2$ has a large unit cell and many inequivalent sites, the band structure of $\text{CaCu}_{1.75}\text{As}_2$ would contain many more bands and the band dispersion (in terms of the reciprocal lattice vectors) would be less comparable to that of the other two copper pnictides. Since the electronic DOS of CaCu_2As_2 is essentially the same as that of $\text{CaCu}_{1.75}\text{As}_2$ (apart from the obvious increase in the

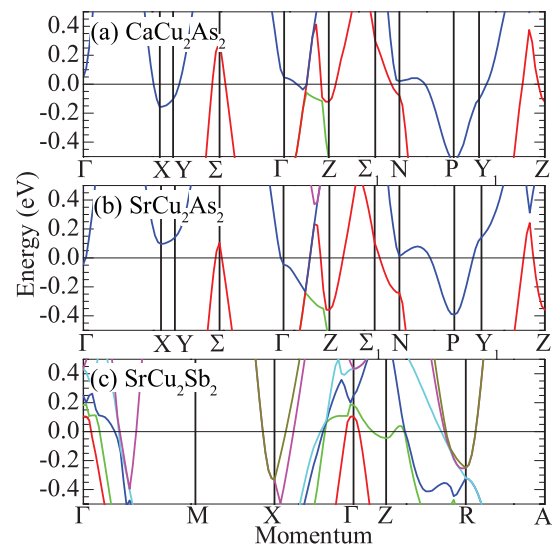


FIG. 5. (Color online) The band structure for (a) CaCu_2As_2 (note the perfect stoichiometry of Cu in this case), (b) SrCu_2As_2 , and (c) SrCu_2Sb_2 near the Fermi level (at 0 eV). Each band is shown in a different color. The high symmetry points for each Brillouin zone are labeled (according to the nomenclature found in Ref. 51), and the corresponding crystal momentum wave numbers have been suppressed for clarity. Note that the paths taken through the Brillouin zone for each system cross the Γ point twice, so the dispersion outwards from the Γ point in three different directions is shown. Note also that the Z point is crossed twice in (a) and (b).

contribution of Cu states to the total DOS), using the simpler stoichiometric CaCu_2As_2 to look at trends in the band structure and Fermi surface is somewhat justified. We should also note that the band structure of SrCu_2As_2 has been previously reported;¹⁴ herein we use a slightly different path through the first Brillouin zone. Both CaCu_2As_2 and SrCu_2As_2 have hole pockets at the Σ point, although this pocket is very small in SrCu_2As_2 . CaCu_2As_2 has a large electron pocket near the X point, while SrCu_2As_2 does not. Both systems have a rather complicated electron pocket at the Γ point. SrCu_2Sb_2 also has an electron pocket at the X point, but there is a hole pocket at the Γ point. The Fermi level of SrCu_2Sb_2 also has many more bands than SrCu_2As_2 (as expected due to the greater number of inequivalent sites and the lower symmetry of the unit cell).

The Fermi surfaces for these materials are shown in Fig. 6. Again note that the Fermi surface of SrCu_2As_2 was previously reported by Singh (also note that in our plots the Γ point is in the center of the figure, while in Singh's plots the Γ point is at the corners).¹⁴ As noted by Singh, the Fermi surfaces of these materials are very three dimensional,¹⁴ in contrast to the largely two-dimensional character of the Fermi surfaces in iron pnictides.^{52–54} The Fermi surface of CaCu_2As_2 is formed by three bands, while the Fermi surface of SrCu_2As_2 is formed by only two. It is possible that the reason why $\text{CaCu}_{1.7}\text{As}_2$ has a significant concentration of Cu vacancies is because reducing the amount of Cu, and consequently reducing the Fermi energy (since the number of electrons in the system is reduced), would dramatically simplify the topology of the Fermi surface.

The Fermi surface of SrCu_2Sb_2 involves 6 different bands, and is also quite three-dimensional [see Fig. 6(c)]. However unlike the copper arsenides, the Fermi surface of SrCu_2Sb_2 is much more cylindrical, like the Fermi surfaces of iron

pnictides. In particular, there are two bands in the Fermi surface of SrCu_2Sb_2 that are almost entirely two dimensional, and this raises the possibility of efficient Fermi surface nesting in this material. Since Fermi surface nesting plays an important role in the properties of iron pnictides,^{3,55} it is perhaps worth investigating SrCu_2Sb_2 under high pressure or after substituting Cu with another transition metal.

F. Conclusions

We have studied the electronic structure of several copper pnictides with soft x-ray spectroscopy measurements and DFT calculations. Our measurements verify the theoretical prediction that the Cu $3d$ -states are fully occupied and deep within the valence band.¹⁴ It seems likely that simple DFT calculations underestimate the binding energy of the Cu $3d^{10}$ shell, probably as a result of DFT's reliance on an approximate exchange functional, but these calculations also possibly underestimate the amount of Cu $3d$ -As $4p$ hybridization. However, in general, simple DFT calculations are quite adequate to explain our measured XES and XAS spectra in these copper pnictides, especially since these minor discrepancies occur at the bottom of the valence band, quite far from the Fermi surface. The shape of the x-ray spectra and the $L_2:L_3$ ratio indicate that copper pnictides, like iron pnictides, are quite metallic and lack strong on-site electron correlations. The degree to which the Cu L_3 XES spectra of these pnictides resembles that of copper metal parallels the trend in $L_2:L_3$ ratio, and qualitatively agrees with the trend in the measured room-temperature conductivity.

To our knowledge this is the first time the electronic structure of several of these copper pnictides have been reported (BaCu_2Sb_2 , SrCu_2Sb_2 , and $\text{CaCu}_{2-x}\text{As}_2$), but like the iron pnictides the specific choice of cation and pnictogen has only a minor influence on the general trends in the electronic structure—so all of our calculated electronic DOSs are quite reminiscent of those from the copper pnictides available in the literature.¹⁴ While the Fermi surfaces of the copper arsenides are quite three dimensional and typical of sp metals,¹⁴ the Fermi surface of SrCu_2Sb_2 has some two-dimensional sheets which could allow efficient Fermi surface nesting to occur. However we should also mention that the band dispersion in SrCu_2Sb_2 is somewhat greater than that in SrFe_2As_2 ,⁵⁶ which leads to a lighter effective mass in the copper pnictide. Therefore the Fermi surface nesting, measured by the Lindhard function in the single-particle limit,⁵⁷ could be less than that in iron pnictides.^{58,59}

Finally, we would like to mention that while it is commonly stated that Cu-substituted iron pnictides and copper pnictides consist of Cu^{1+} sites,^{13,20,22,23} our XAS measurements suggest that a formal Cu^{1+} ion is not present. In Cu_2O , a typical Cu^{1+} system, hybridization between the O $2p$ -Cu $3d$ valence states introduces significant $3d$ character in the conduction band which manifests as a large $2p \rightarrow 3d$ resonance in the Cu $L_{2,3}$ XAS.⁶⁰ The fact that this resonance is completely absent from our XAS measurements and there is plenty of hybridization between the pnictogen s,p Cu $3d$ valence states suggests that it may be appropriate to view the entire pnictogen-Cu layer as a metal; identifying the copper atoms as Cu^{1+} should be interpreted in the sense that the Cu $4s$ states are itinerant, not

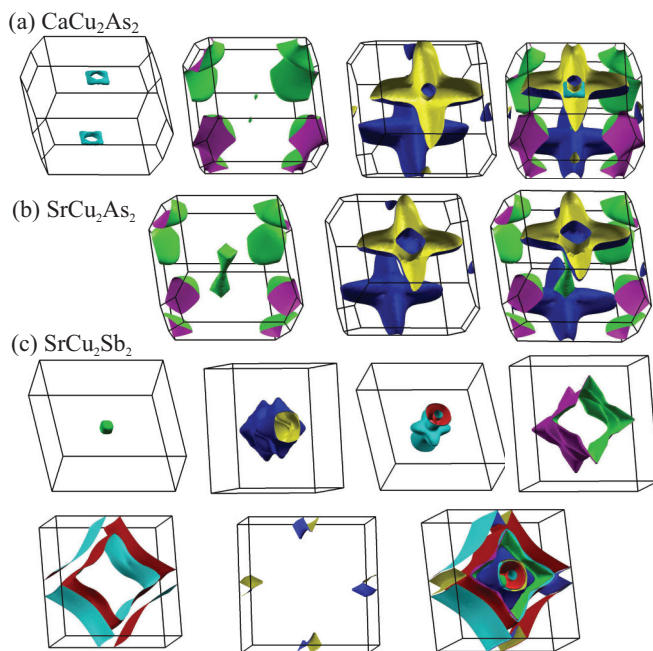


FIG. 6. (Color online) The Fermi surfaces for (a) CaCu_2As_2 (note the perfect stoichiometry of Cu in this case), (b) SrCu_2As_2 , and (c) SrCu_2Sb_2 . Each band is shown separately; the complete Fermi surface is shown to the bottom right for each system.

that the copper is acting as a formal cation in Cu-pnictogen bonding.

ACKNOWLEDGMENTS

We gratefully acknowledge support from the Natural Sciences and Engineering Research Council of Canada (NSERC) and the Canada Research Chair program. This work was done with partial support of the Ural Division of the Russian Academy of Sciences (Project No. 12-I-2-2040). The Advanced Light Source is supported by the Director, Office of Science, Office of Basic Energy Sciences, of the US Department of Energy under Contract No. DE-AC02-

05CH11231. The Canadian Light Source is supported by NSERC, the National Research Council (NSC) Canada, the Canadian Institute of Health Research (CIHR), the Province of Saskatchewan, Western Economic Diversification Canada, and the University of Saskatchewan. The computational part of this research was enabled by the use of computing resources provided by WestGrid and Compute/Calcul Canada. The work at Ames Laboratory was supported by the US Department of Energy, Office of Basic Energy Sciences, Division of Materials Sciences and Engineering. Ames Laboratory is operated for the US Department of Energy by Iowa State University under Contract No. DE-AC02-07CH11358.

*Corresponding author: john.mcleod@usask.ca

- ¹Y. Kamihara, T. Watanabe, M. Hirano, and H. Hosono, *J. Am. Chem. Soc.* **130**, 3296 (2008).
- ²D. C. Johnston, *Adv. Phys.* **59**, 803 (2010).
- ³S. A. J. Kimber, A. Kreyssig, Y.-Z. Zhang, H. O. Jeschke, R. Valentí, F. Yokaichiya, E. Colombier, J. Yan, T. C. Hansen, T. Chatterji, R. J. McQueeney, P. C. Canfield, A. I. Goldman, and D. N. Argyriou, *Nat. Mater.* **8**, 471 (2009).
- ⁴N. Ni, A. Thaler, J. Q. Yan, A. Kracher, E. Colombier, S. L. Bud'ko, P. C. Canfield, and S. T. Hannahs, *Phys. Rev. B* **82**, 024519 (2010).
- ⁵A. Olariu, F. Rullier-Albenque, D. Colson, and A. Forget, *Phys. Rev. B* **83**, 054518 (2011).
- ⁶N. Ni, S. L. Bud'ko, A. Kreyssig, S. Nandi, G. E. Rustan, A. I. Goldman, S. Gupta, J. D. Corbett, A. Kracher, and P. C. Canfield, *Phys. Rev. B* **78**, 014507 (2008).
- ⁷A. S. Sefat, R. Jin, M. A. McGuire, B. C. Sales, D. J. Singh, and D. Mandrus, *Phys. Rev. Lett.* **101**, 117004 (2008).
- ⁸J.-T. Han, J.-S. Zhou, J.-G. Cheng, and J. B. Goodenough, *J. Am. Chem. Soc.* **132**, 908 (2010).
- ⁹A. F. Kemper, C. Cao, P. J. Hirschfeld, and H.-P. Cheng, *Phys. Rev. B* **80**, 104511 (2009).
- ¹⁰E. M. Bittar, C. Adriano, T. M. Garitezi, P. F. S. Rosa, L. Mendonça-Ferreira, F. Garcia, G. d. M. Azevedo, P. G. Pagliuso, and E. Granado, *Phys. Rev. Lett.* **107**, 267402 (2011).
- ¹¹P. C. Canfield, S. L. Bud'ko, N. Ni, J. Q. Yan, and A. Kracher, *Phys. Rev. B* **80**, 060501(R) (2009).
- ¹²H. Wadati, I. Elfimov, and G. A. Sawatzky, *Phys. Rev. Lett.* **105**, 157004 (2010).
- ¹³J. A. McLeod, A. Buling, R. J. Green, T. D. Boyko, N. A. Skorikov, E. Z. Kurmaev, M. Neumann, L. D. Finkelstein, N. Ni, A. Thaler, S. L. Bud'ko, P. C. Canfield, and A. Moewes, *J. Phys.: Condens. Matter* **24**, 215501 (2012).
- ¹⁴D. J. Singh, *Phys. Rev. B* **79**, 153102 (2009).
- ¹⁵E. Z. Kurmaev, J. A. McLeod, A. Buling, N. A. Skorikov, A. Moewes, M. Neumann, M. A. Korotin, Y. A. Izyumov, N. Ni, and P. C. Canfield, *Phys. Rev. B* **80**, 054508 (2009).
- ¹⁶T. Yildirim, *Phys. Rev. Lett.* **102**, 037003 (2009).
- ¹⁷V. I. Anisimov, E. Z. Kurmaev, A. Moewes, and I. A. Izyumov, *Physica C* **469**, 442 (2009).
- ¹⁸M. Aichhorn, L. Pourovskii, V. Vildosola, M. Ferrero, O. Parcollet, T. Miyake, A. Georges, and S. Biermann, *Phys. Rev. B* **80**, 085101 (2009).

- ¹⁹J. A. McLeod, R. G. Wilks, N. A. Skorikov, L. D. Finkelstein, M. Abu-Samak, E. Z. Kurmaev, and A. Moewes, *Phys. Rev. B* **81**, 245123 (2010).
- ²⁰S. Ideta, T. Yoshida, I. Nishi, A. Fujimori, Y. Kotani, K. Ono, Y. Nakashima, S. Yamaichi, T. Sasagawa, M. Nakajima, K. Kihou, Y. Tomioka, C. H. Lee, A. Iyo, H. Eisaki, T. Ito, S. Uchida, and R. Arita, *Phys. Rev. Lett.* **110**, 107007 (2013).
- ²¹I. I. Mazin, M. D. Johannes, L. Boeri, K. Koepernik, and D. J. Singh, *Phys. Rev. B* **78**, 085104 (2008).
- ²²V. K. Anand and D. C. Johnston, *Phys. Rev. B* **86**, 214501 (2012).
- ²³V. K. Anand, P. K. Perera, A. Pandey, R. J. Goetsch, A. Kreyssig, and D. C. Johnston, *Phys. Rev. B* **85**, 214523 (2012).
- ²⁴J. J. Jia, T. A. Callcott, J. Yurkas, A. W. Ellis, and F. J. Himpsel, *Rev. Sci. Instrum.* **66**, 1394 (1995).
- ²⁵T. Regier, J. Krochak, T. K. Sham, Y. F. Hu, J. Thompson, and R. I. R. Blyth, *Nucl. Instrum. Methods Phys. Res., Sect. A* **582**, 93 (2007).
- ²⁶The actual basis was a mixture of the “augmented plane wave plus local orbitals” basis (APW + lo) for chemically relevant states (up to d states for Cu and the pnictogens, up to p states for the alkaline metals), and the LAPW basis for states with higher angular momenta; additional local orbitals (LOs) were added for the appropriate semicore states (i.e., the Cu $3p$ states). All of these choices are WIEN2k’s default selections for each particular atomic species.
- ²⁷P. Blaha, K. Schwarz, G. K. H. Madsen, D. Kvasnicka, and J. Luitz, *WIEN2k, An Augmented Plane Wave + Local Orbitals Program for Calculating Crystal Properties* (Karlheinz Schwarz, Techn. Universität Wien, Austria, 2001).
- ²⁸Energy convergence of 0.0001 Ryd, charge convergence of 0.001 e , the Brillouin zone discretized on a 1000-element k -point grid, and $P_{\min}^{MT} K_{\max} = 7$. The atomic sphere radii were chosen so that the spheres were nearly touching; the radii were 2.5 bohrs, 2.42 bohrs, 2.29 bohrs, and 2.15 bohrs for the alkaline metals (Ca, Sr, and Ba), Cu, Sb, and As, respectively. The cutoff between core and valence states was -6 Ryd. See our previous papers for more details (Refs. 13 and 15).
- ²⁹J. P. Perdew, K. Burke, and M. Ernzerhof, *Phys. Rev. Lett.* **77**, 3865 (1996).
- ³⁰H. M. Otte, *J. Appl. Phys.* **32**, 1536 (1961).
- ³¹S. Asbrink and L. J. Norrby, *Acta. Cryst. B* **26**, 8 (1970).

- ³²J.-M. Mariot, V. Barnole, C. Hague, G. Vetter, and F. Queyroux, *Z. Phys. B: Condens. Matter* **75**, 1 (1989).
- ³³J. Ghijsen, L. H. Tjeng, J. van Elp, H. Eskes, J. Westerink, G. A. Sawatzky, and M. T. Czyzyk, *Phys. Rev. B* **38**, 11322 (1988).
- ³⁴J. Ghijsen, L. H. Tjeng, H. Eskes, G. A. Sawatzky, and R. L. Johnson, *Phys. Rev. B* **42**, 2268 (1990).
- ³⁵H. Eskes, L. H. Tjeng, and G. A. Sawatzky, *Phys. Rev. B* **41**, 288 (1990).
- ³⁶K. Schwarz, A. Neckel, and J. Nordgren, *J. Phys. F: Metal Phys.* **9**, 2509 (1979).
- ³⁷D. A. Goodings and R. Harris, *J. Phys. C: Solid State Phys.* **2**, 1808 (1969).
- ³⁸J. Dünner, A. Mewis, M. Roepke, and G. Michels, *Z. Anorg. Allg. Chem.* **621**, 1523 (1995).
- ³⁹W. L. Yang *et al.*, *Phys. Rev. B* **80**, 014508 (2009).
- ⁴⁰V. Mauchamp, M. Jaouen, and P. Schattschneider, *Phys. Rev. B* **79**, 235106 (2009).
- ⁴¹E. Z. Kurmaev, R. G. Wilks, A. Moewes, L. D. Finkelstein, S. N. Shamin, and J. Kuneš, *Phys. Rev. B* **77**, 165127 (2008).
- ⁴²F. de Groot, *Coordin. Chem. Rev.* **249**, 31 (2005).
- ⁴³The additional shifts needed to “correct” the energy alignment of the calculated XES L_3 spectra taken with respect to the calculated binding energy of the Cu $2p_{3/2}$ core levels were 3.5 eV for BaCu₂As₂, SrCu₂As₂, and SrCu₂(As_{0.875}Sb_{0.125})₂; 3.6 eV for Cu metal; and 3.7 eV for SrCu₂Sb₂ and CaCu_{1.75}As₂.
- ⁴⁴C. L. Dong, C. Persson, L. Vayssieres, A. Augustsson, T. Schmitt, M. Mattesini, R. Ahuja, C. L. Chang, and J.-H. Guo, *Phys. Rev. B* **70**, 195325 (2004).
- ⁴⁵J. E. Jaffe and A. C. Hess, *Phys. Rev. B* **48**, 7903 (1993).
- ⁴⁶M. O. Krause, *J. Phys. Chem. Ref. Data* **8**, 307 (1979).
- ⁴⁷E. Z. Kurmaev, A. L. Ankudinov, J. J. Rehr, L. D. Finkelstein, P. F. Karimov, and A. Moewes, *J. Electron Spectrosc. Relat. Phenom.* **148**, 1 (2005).
- ⁴⁸C. F. Hague, J.-M. Mariot, G. Y. Guo, K. Hricovini, and G. Krill, *Phys. Rev. B* **51**, 1370 (1995).
- ⁴⁹E. Z. Kurmaev, R. G. Wilks, A. Moewes, N. A. Skorikov, Y. A. Izyumov, L. D. Finkelstein, R. H. Li, and X. H. Chen, *Phys. Rev. B* **78**, 220503(R) (2008).
- ⁵⁰E. Z. Kurmaev, J. A. McLeod, N. A. Skorikov, L. D. Finkelstein, A. Moewes, Y. A. Izyumov, and S. Clarke, *J. Phys.: Condens. Matter* **21**, 345701 (2009).
- ⁵¹W. Setyawan and S. Curtarolo, *Comput. Mater. Sci.* **49**, 299 (2010).
- ⁵²P. A. Lee and X.-G. Wen, *Phys. Rev. B* **78**, 144517 (2008).
- ⁵³K. Kuroki, S. Onari, R. Arita, H. Usui, Y. Tanaka, H. Kontani, and H. Aoki, *Phys. Rev. Lett.* **101**, 087004 (2008).
- ⁵⁴A. Subedi, L. Zhang, D. J. Singh, and M. H. Du, *Phys. Rev. B* **78**, 134514 (2008).
- ⁵⁵K. Terashima, Y. Sekiba, J. H. Bowen, K. Nakayama, T. Kawahara, T. Sato, P. Richard, Y.-M. Xu, L. J. Li, G. H. Cao, Z.-A. Xu, H. Ding, and T. Takahashi, *Proc. Natl. Acad. Sci. USA* **106**, 7330 (2009).
- ⁵⁶Y. Zhang, J. Wei, H. W. Ou, J. F. Zhao, B. Zhou, F. Chen, M. Xu, C. He, G. Wu, H. Chen, M. Arita, K. Shimada, H. Namatame, M. Taniguchi, X. H. Chen, and D. L. Feng, *Phys. Rev. Lett.* **102**, 127003 (2009).
- ⁵⁷D. Bergeron, D. Chowdhury, M. Punk, S. Sachdev, and A.-M. S. Tremblay, *Phys. Rev. B* **86**, 155123 (2012).
- ⁵⁸C. Parks Cheney, F. Bondino, T. A. Callcott, P. Vilmercati, D. Ederer, E. Magnano, M. Malvestuto, F. Parmigiani, A. S. Sefat, M. A. McGuire, R. Jin, B. C. Sales, D. Mandrus, D. J. Singh, J. W. Freeland, and N. Mannella, *Phys. Rev. B* **81**, 104518 (2010).
- ⁵⁹D. S. Inosov, V. B. Zabolotnyy, D. V. Evtushinsky, A. A. Kordyuk, B. Büchner, R. Follath, H. Berger, and S. V. Borisenko, *New J. Phys.* **10**, 125027 (2008).
- ⁶⁰J. P. Hu, D. J. Payne, R. G. Egdell, P.-A. Glans, T. Learmonth, K. E. Smith, J. Guo, and N. M. Harrison, *Phys. Rev. B* **77**, 155115 (2008).